Nano Energy 49 (2018) 580–587

Contents lists available at ScienceDirect

Nano Energy

journal homepage: www.elsevier.com/locate/nanoen

Full paper

Boosting interfacial Li^+ transport with a MOF-based ionic conductor for solid-state batteries

Ziqi Wang[1], Zijian Wang[1], Luyi Yang, Hongbin Wang, Yongli Song, Lei Han, Kai Yang, Jiangtao Hu, Haibiao Chen, Feng Pan*

School of Advanced Materials, Peking University Shenzhen Graduate School, Shenzhen 518055, PR China

ARTICLE INFO

Keywords:
Ionic conductors
Interfacial Li^+ transports
Nanowetted interfaces
Solid-state batteries

ABSTRACT

Concerning the large interfacial resistance of materials within solid-stated batteries (SSBs) caused by the unstable solid contact, an assistant ionic conductor is introduced to improve the interfacial Li^+ transport of SSBs. The assistant ionic conductor is achieved by impregnating an ionic liquid (Li-IL) into a porous metal-organic framework (MOF) host. When integrated with LLZO solid-state electrolyte (SSE), the solidified Li-IL guest can make direct contact with the LLZO particles through the open channels in MOF host, which changes the original unstable solid-solid contact into "nanowetted" interfaces to boost Li^+ transport. Benefited from the unique nanowetted interfaces, the hybrid SSE demonstrates a high ionic conductivity of 1.0×10^{-4} S cm^{-1} with a wide electrochemical window of 5.2 V, and also exhibits excellent compatibility with Li metal anode. Furthermore, the LLZO based $LiCoO_4$ and $LiFePO_4$ SSBs with the ionic conductor additive to favor the interfacial Li^+ transport achieve high capacity retention of 97% after 150 cycles with reasonable rate capability. The good electrochemical performance is attributed to the effective Li^+ transport networks established inside the SSBs by the ionic conductor through the nanowetted interfacial mechanism, which is proved to be a promising approach to the safe and high-power energy storage.

1. Introduction

Lithium-ion batteries (LIBs) have dominated the market of portable electronic devices over the past two decades [1,2], but the low energy density and the safety issues like leakage and fire concerned with liquid organic electrolytes make LIBs difficult to satisfy the demand of high-power applications such as electronic vehicles and grid energy storage [3,4]. Solid-state batteries (SSBs) which replace liquid organic electrolytes with safer solid-state electrolytes (SSEs) and directly use high-capacity lithium metal anode, are considered to be promising candidates for future energy storage [5–7]. However, due to the rigid and brittle nature of the ceramic SSEs, the interfacial issue is a great challenge hindering the practical application of SSBs [8,9]. Li^+ transport kinetics across the solid-solid interfaces (both between SSE particles and SSE-electrode interfaces) is much poor compared with that of traditional LIBs with liquid-solid interfaces, thus limiting the active loading and the rate capability of SSBs. Targeting the interfacial problem, many efforts have been made in recent years. Taking garnet $Li_7La_3Zr_2O_{12}$ (LLZO) SSE as an example, the interpaticle structure of the LLZO grains can be optimized through a post-sintering treatment to achieve a high bulk ionic conductivity, but such a strategy was proven inapplicable to the heterogeneous SSE-electrode interfaces due to the poor interface match and the harsh processing conditions [10–12]. The poor contact interfaces between LLZO and Li metal anode can be ameliorated by introducing an artificial transition layer such as Al [13], Al_2O_3 [14], or ZnO [15] to boost the Li^+ transport. However, some liquid organic electrolytes were still needed in the cathode region to realize a normal battery performance, and thus the safety risks of fire and volatilization still remain. Therefore, it is urgent and meaningful to explore new strategies to solve the interfacial issue.

Additional ionic conductors at the interfaces of SSBs may help to promote the interfacial Li^+ transport kinetics and the metal-organic frameworks (MOFs) are excellent platforms for building ionic conductors because they are electrical insulators with highly tunable porous structure for fast ion movement [16]. Li^+ conductive MOFs were firstly reported by Long's group and their Mg-MOF-74 [17] and UIO-66 [18] based materials demonstrated a conductivity of 3.1×10^{-4} S cm^{-1} and 1.8×10^{-5} S cm^{-1} at room temperature, respectively. In 2015, Kitagawa [19] and co-workers developed a Li^+ conductive ZIF-8 by filling its pores with ionic liquids. Recently, Dincă

* Corresponding author.
E-mail address: panfeng@pkusz.edu.cn (F. Pan).
[1] These authors contributed equally to this work.

https://doi.org/10.1016/j.nanoen.2018.04.076
Received 8 March 2018; Received in revised form 18 April 2018; Accepted 30 April 2018
Available online 01 May 2018

[16] and co-workers reported a series of single-ion conductors based on the post-synthetic modified MIT-20. Despite much progress has been made, due to the conductivity and the electrochemical stability issues, the application of MOF electrolytes in real batteries is still hard to realize. Earlier this year we first used MOF-525 based electrolyte in the $LiFePO_4$ SSBs and achieved stable cycling performance [12], but its electrochemical window was too narrow (2–4.1 V) due to the redox-active Cu(II) centers, which was not applicable to the high-voltage layered oxide cathodes.

In this work, we designed a novel electrochemically stable MOF ionic conductor, which was applied to the LLZO-based SSBs to effectively promote the interfacial Li^+ transport kinetics. The assistant ionic conductor (LI-IL@MOF, named as LIM) was a host-guest composite of a porous MOF and a Li^+ containing ionic liquid (Li-IL). The Li-IL guest was solidified by being encapsulated into the pores of MOF host, and preserved its high ionic conductivity without forming external liquid phase. As an ionic conductive agent for SSBs, LIM provided abundant direct contact points through its 3D opening crystal structure for the LLZO and the cathode particles with the inside Li-IL ions at atomic scale, which turned the primitive solid-solid contact into "nanowetted" interfaces to decrease the interfacial resistance of the SSBs significantly. Without a sintering procedure, by simply mixing LLZO powders with 20 wt% LIM, the hybrid SSE (LI-IL@MOF-LLZO named as LIM-L) demonstrated a high ionic conductivity of 1.0×10^{-4} S cm^{-1} with a wide electrochemical window of 5.2 V at room temperature, and also exhibited excellent compatibility with Li metal anode. When the LIM ionic conductor was introduced to the $LiCoO_2$ (LCO) and $LiFePO_4$ (LFP) SSBs, efficient Li^+ transport networks could be established inside the batteries, leading to stable cyclability with acceptable rate capability at very high active loadings of 15.9 and 12.4 mg cm^{-2}, respectively.

2. Experimental section

2.1. Materials

UIO-67. UIO-67 was synthesized according to the reported procedures [20] with a little modification. Typically, 80 mg 4,4′-biphenyldicarboxylic acid (BPDC) ligand was dissolved in 30 mL N,N-dimethylformamide (DMF) and then 0.54 mL triethylamine was added to the ligand solution. For the metal solution, 80 mg $ZrCl_4$ with 3.4 mL acetic acid was dissolved in 24 mL DMF. The two solutions were mixed and stirred at room temperature into a homogeneous solution which was loaded in a 100 mL autoclave and heated at 85 °C for 24 h. UIO-67 was collected by centrifuging and washed with methanol and then activated by heating at 120 °C in dynamic vacuum overnight. The activated UIO-67 was stored in an Ar glove-box for further use.

2.1.1. LIM ionic conductor

0.223 g LiTFSI was dissolved in 1 mL [EMIM][TFSI] obtaining Li-IL ionic liquid, which was heated at 120 °C overnight before use. Different amount of Li-IL was added to the activated UIO-67 separately, milled into homogeneous mixtures and heated at 120 °C in the vacuum overnight to obtain LIM ionic conductor. All the above procedures were carried out in an Ar glove-box. The LIM pellet for the electrochemical tests were prepared by pressing the LIM powder into a pellet with a diameter of 1.2 cm under 8 T force.

2.1.2. LLZO

Cubic phase LLZO powder with Al^{3+} doping ($Li_{6.25}Al_{0.25}La_3Zr_2O_{12}$) was prepared according to the procedure reported elsewhere [21]. Typically, $LiOH{\cdot}H_2O$, $La(OH)_3$, ZrO_2, and Al_2O_3 with the molar ratio of 7.7: 3: 2: 0.25 were mixed by ball milling in a speed of 400 r min^{-1} for 8 h. The mixture was then sintered at 950 °C for 8 h in a ZrO_2 crucible to produce the LLZO powder. For electrochemical tests, LLZO powder was pressed into a 1.2 cm pellet under 8 T force. The sintered LLZO pellet was prepared by sintering the pristine LLZO pellet buried in LLZO powder at 1100 °C for 5 h. The sintered LLZO pellet was polished before test.

2.1.3. LIM-L hybrid SSE

LIM-L hybrid SSE was prepared by mixing LLZO powder with different amounts of LIM ionic conductor in an Ar glove-box which was then pressed into 1.2 cm pellet under 8 T force for the electrochemical tests.

2.1.4. Battery assembling

Commercial LCO, LIM, and acetylene black were mixed in the weight ratio of 5: 4: 1 as the cathode mixture. 16 mg cathode mixture was pressed into a 0.8 cm pellet under 3 T force, and then pressed sequentially with another 60 mg LIM-L into a 1.2 cm bilayer pellet under 8 t force. Solid-state batteries were assembled in Ar glove-box and tested in Swagelok cells using Li foil as anode and the bilayer pellet as cathode and separator. Similar procedures were followed to assemble the LFP SSB except that the cathode composition was 5: 5: 2 and 15 mg cathode mixture with 55 mg LIM-L hybrid SSE were used for the bilayer pellet.

2.2. Methods

Powder X-ray diffraction (XRD) data were recorded by a Bruker D8 Advance diffractometer using Cu Kα, λ = 1.541 Å. The scanning electron microscopy (SEM) morphology and energy dispersive spectrometer (EDS) mapping were investigated using ZEISS Supra 55 scanning electron microscopy with an Oxford AZtec energy dispersive spectrometer. N_2 adsorption-desorption isothermal was recorded on a Micromeritics ASAP 2020 HD88 tool. Thermo gravimetric analysis (TGA) was carried out in a N_2 atmosphere at a scan speed of 10 °C min^{-1} on a Mettler Toledo TGA/DSC STAR system. X-ray photoelectron spectroscopy (XPS) analysis was performed on an ESCALAB 250XL instrument in a scan step of 0.1 eV. The cyclic voltammetry (CV, 0.2 mV s^{-1}), linear sweep voltammetry (LSV, 0.2 mV s^{-1}) and electrochemical impedance spectroscopy (EIS, 1–1 M Hz) data were collected with a CHI600E electrochemical workstation. The Li plating-stripping cycles and battery cycling performance were obtained with a LAND battery cycler.

3. Results and discussion

The constructional details and working mechanism of the SSB with LIM as ionic conductive agent are illustrated Scheme 1. UIO-67 [22] constructed by $Zr_6(IV)O_4(OH)_4$ nodes and biphenyl-4,4′-dicarboxylic acid (BPDC) linkers was used as the solid MOF host considering its high porosity, proper pore size (about 12 Å for each octahedral cage), and excellent chemical stability. Nano-sized UIO-67 crystals were synthesized following the established procedure [20] with a little modification, and their phase purity was confirmed by the X-ray diffraction (XRD) pattern which was well consistent with the simulated one based on the reported crystal structure, as shown in Fig. 1**a**. Scanning electron microscopy (SEM) image in Fig. 1**c** suggested that the as-prepared UIO-67 crystals were 80–150 nm in size with a spherical shape. An imidazolium-based ionic liquid electrolyte (0.8 M LiTFSI in [EMIM][TFSI], where TFSI is bis(trifluoromethylsulfonyl)amide and EMIM is 1-ethyl-3-methylimidazolium.) was selected as the Li^+ conductive guest (Li-IL) for its high ionic conductivity, low vapor pressure, low viscosity, and wide electrochemical window [23,24]. As the Li-IL content in LIM directly determines its ionic conductivity [19], the optimal loading amount of Li-IL should be identified before other tests. A series of LIM ionic conductors was prepared through mixing the activated MOF host with different amounts of Li-IL guest in an Ar filled glovebox followed by a heating process in vacuum to assist Li-IL impregnation. These LIM samples were mechanically pressed into pellets afterwards and sandwiched between two silver coated stainless steel electrodes for conductivity tests. Arrhenius plots for the ionic conductivity are shown in

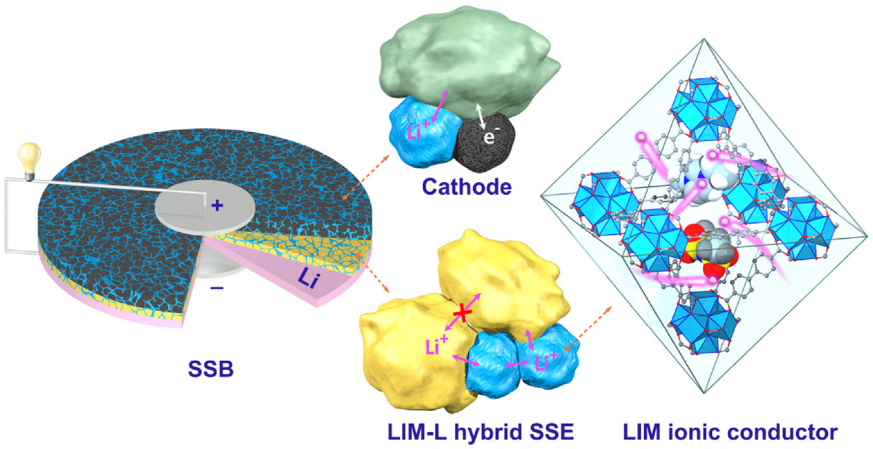

Scheme 1. Schematic illustration for the architecture of the solid-state battery with LIM ionic conductive agent and its working mechanism. The particles with green, yellow, blue, and black color represent the cathode material, LLZO, LIM, and conductive carbon, respectively. $Zr_6(IV)O_4(OH)_4$ clusters in UIO-67 are shown by blue polyhedrons. The migrating Li^+ ions are highlighted by the glowing pink spheres and the $[EMIM]^+$ and $[TFSI]^-$ ions are randomly distributed in the pores of UIO-67 in Space-Filling model. Hydrogen atoms are omitted in the UIO-67 structure for clarity.

Fig. 2**a**, and the values of 1.46×10^{-5}, 1.14×10^{-4}, 3.12×10^{-4}, and 8.71×10^{-4} S cm^{-1} were observed at 30 °C for the samples of 1.0 g MOF host impregnated with 0.5, 1.0, 1.5, and 2.0 mL Li-IL guest, respectively. With the content of Li-IL growing, the ionic conductivity of LIM rose up as a result of the increasing ion conductive paths inside the MOF host, and the highest conductivity close to that of pristine Li-IL electrolyte [19,25] was achieved with 2.0 mL Li-IL addition. However, this sample took on a wet-gel state indicating an excess amount of liquid Li-IL which could not be absorbed by the MOF host. The other three composites with Li-IL contents less than 1.5 mL were completely solidified and remained as "free-flowing" dry powders (Fig. S1), which could eliminate the risk of liquid leakage. Accordingly, LIM with the optimized composition of 1.0 g MOF: 1.5 mL Li-IL was used in the following experiments, and the electrochemical impedance spectroscopy (EIS) of this sample in the range of 30–100 °C is displayed in Fig. 2**b**. According to the 77 K N_2 adsorption-desorption tests (Fig. S2), the BET surface area of pristine UIO-67 MOF host was 2169 m^2 g^{-1} demonstrating its high porosity, and it dropped to 8 m^2 g^{-1} for the LIM ionic conductor suggesting a high occupation rate of Li-IL guest in the pores of MOF host. The XRD pattern of LIM in Fig. 1**a** shows identical reflection peaks with pristine UIO-67, indicating that the structure of the MOF host was intact after Li-IL uptake and subsequent heating. Drop in

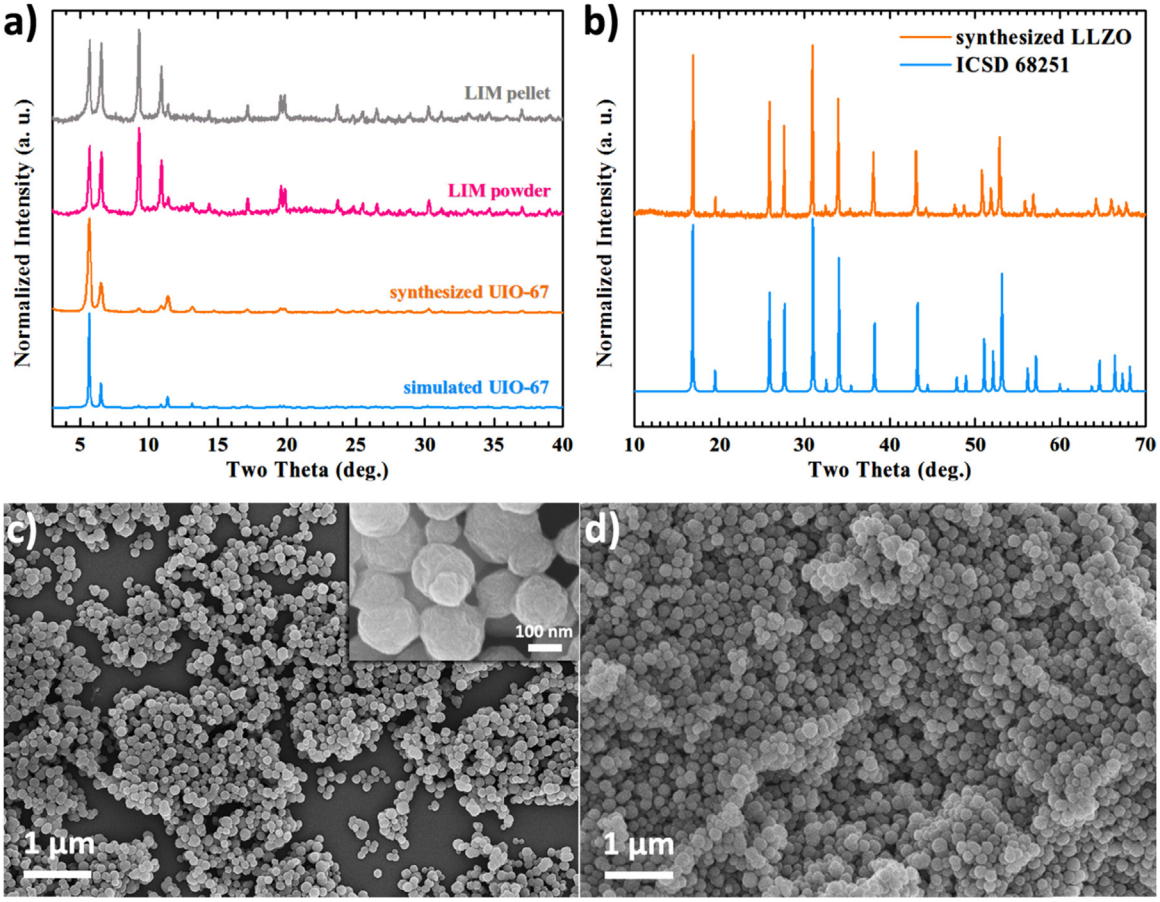

Fig. 1. a) XRD patterns of the synthesized UIO-67 MOF host compared with the simulated result, the LIM ionic conductor and its pellet form pressed under 700 MPa. b) XRD patterns of the synthesized ceramic LLZO powders and the standard $Li_5La_3Nb_2O_{12}$ (ICSD #68251) phase. SEM images of c) the synthesized UIO-67 MOF host and d) the LIM ionic conductor.

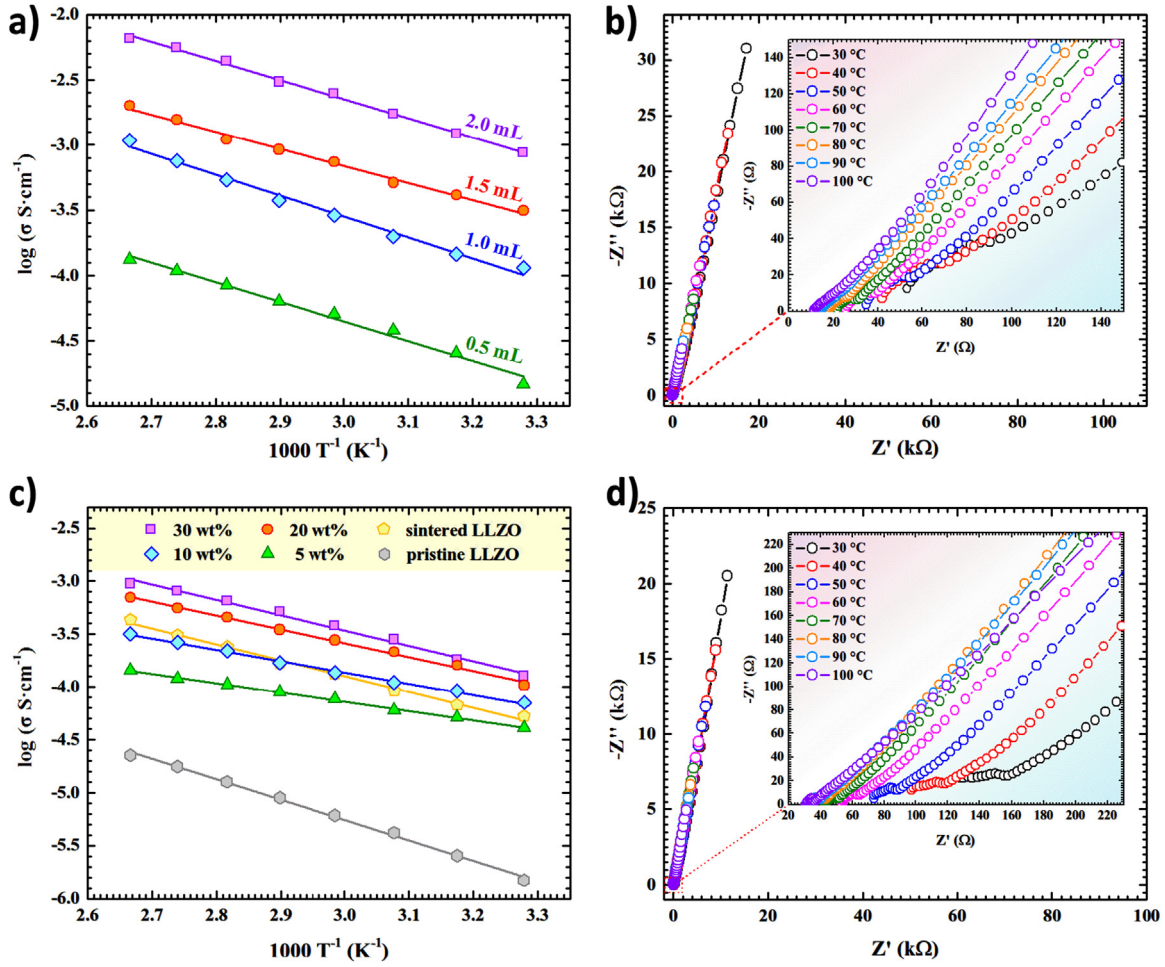

Fig. 2. a) Arrhenius plots for the ionic conductivity of the LIMs with different Li-IL loading amounts. The MOF host in each sample was fixed as 1.0 g. b) EIS within frequency of 1–1 M Hz of the LIM sample with 1.5 mL Li-IL at temperatures from 30° to 100°C, inset: magnified high frequency region. c) Arrhenius plots for the ionic conductivity of the pristine LLZO, the sintered LLZO, and the LIM-L hybrid SSEs with different LIM contents. d) EIS within frequency of 1–1 M Hz of the LIM-L (containing 20 wt% of LIM) at temperatures from 30° to 100°C, inset: magnified high frequency region.

the intensity of the first reflection peak was probably caused by the disordered Li-IL guest ions [26]. The chemical stability of MOF against Li-IL was further proved by the SEM image of LIM, which demonstrated a similar morphology to the pristine UIO-67, as shown in Fig. 1**d**. The crystal structure of LIM was unchanged after being pressed under 700 MPa pressure as proved by the XRD of LIM pellet, demonstrating its high mechanical stability. Thermo-gravimetric analysis (TGA) in N_2 atmosphere was performed on the LIM ionic conductor to examine its thermal stability, and the degradation temperature was over 360 °C as shown in Fig. S3, which promised a wide operating temperature range for SSBs.

LLZO was selected as the main body of the SSE layer because of its high ionic conductivity and Li^+ transference number (t_{Li+} = 1 theoretically) [27]. It can also effectively block Li dendrite growth by virtue of its rigid ceramic nature and good chemical stability against Li metal [28]. Cubic phase LLZO powders with Al^{3+} doping ($Li_{6.25}Al_{0.25}La_3Zr_2O_{12}$) to stabilize the structure were prepared according to the procedure reported elsewhere [21], and the phase purity was confirmed by its XRD pattern in Fig. 1**b**. The synthesized LLZO powders were pressed into pellets and sintered at 1100 °C to perform conductivity test. Arrhenius plots for the ionic conductivity of the LLZO pellet before and after sintering are shown in Fig. 2**c**. The sintered LLZO pellet exhibited a reasonable ionic conductivity of 5.3×10^{-5} S cm^{-1} at 30 °C, while only 1.5×10^{-6} S cm^{-1} was achieved for the pristine LLZO pellet. To understand this, SEM morphologies of the pellets were further investigated. As displayed in Fig. S4, large gaps between LLZO grains can be observed on the pristine LLZO pellet, but the sintered one revealed a much dense packing morphology instead. It thus follows that, the large interfacial resistance caused by the poor grain contact should be responsible for the low conductivity of pristine LLZO pellet and the grain boundary fusion after sintering could effectively promote the interfacial Li^+ transport leading to a higher ionic conductivity. Unfortunately, the sintering process was not applicable to the heterogeneous SSE-electrode interfaces due to the poor interface match and the harsh processing conditions.

As an alternative strategy, LIM ionic conductor was introduced to the LLZO SSE to reduce its interfacial resistance. By simply mixing LLZO powders with different amounts of LIM and pressing into pellet without sintering, a series of LIM-L hybrid SSEs was prepared and tested. As shown in Fig. 2**c**, the pristine LLZO revealed a low conductivity of 1.5×10^{-6} S cm^{-1} at 30 °C, which were increased to 4.1×10^{-5}, 7.1×10^{-5}, 1.0×10^{-4}, and 1.3×10^{-4} S cm^{-1} when 5 wt%, 10 wt%, 20 wt%, and 30 wt% LIM was added, respectively. As another important parameter for electrolyte materials, Li^+ transference number (t_{Li+}) of the LIM-L hybrid SSEs was estimated using a Li|LIM-L|Li symmetric cell by Evans method [29] with a constant polarization potential of 10 mV at room temperature. The comparison of t_{Li+} for different materials is displayed in Fig. 3**b**. As can be seen, the pristine Li-IL electrolyte with the use of a glass fiber separator demonstrated a very low t_{Li+} of 0.11 because the majority of the conducting ions in Li-IL were $[EMIM]^+$ and $[TFSI]^-$ rather than Li^+ [30]. After impregnating the Li-IL into the MOF host, a slightly increased t_{Li+} of 0.13 was observed on LIM, which we

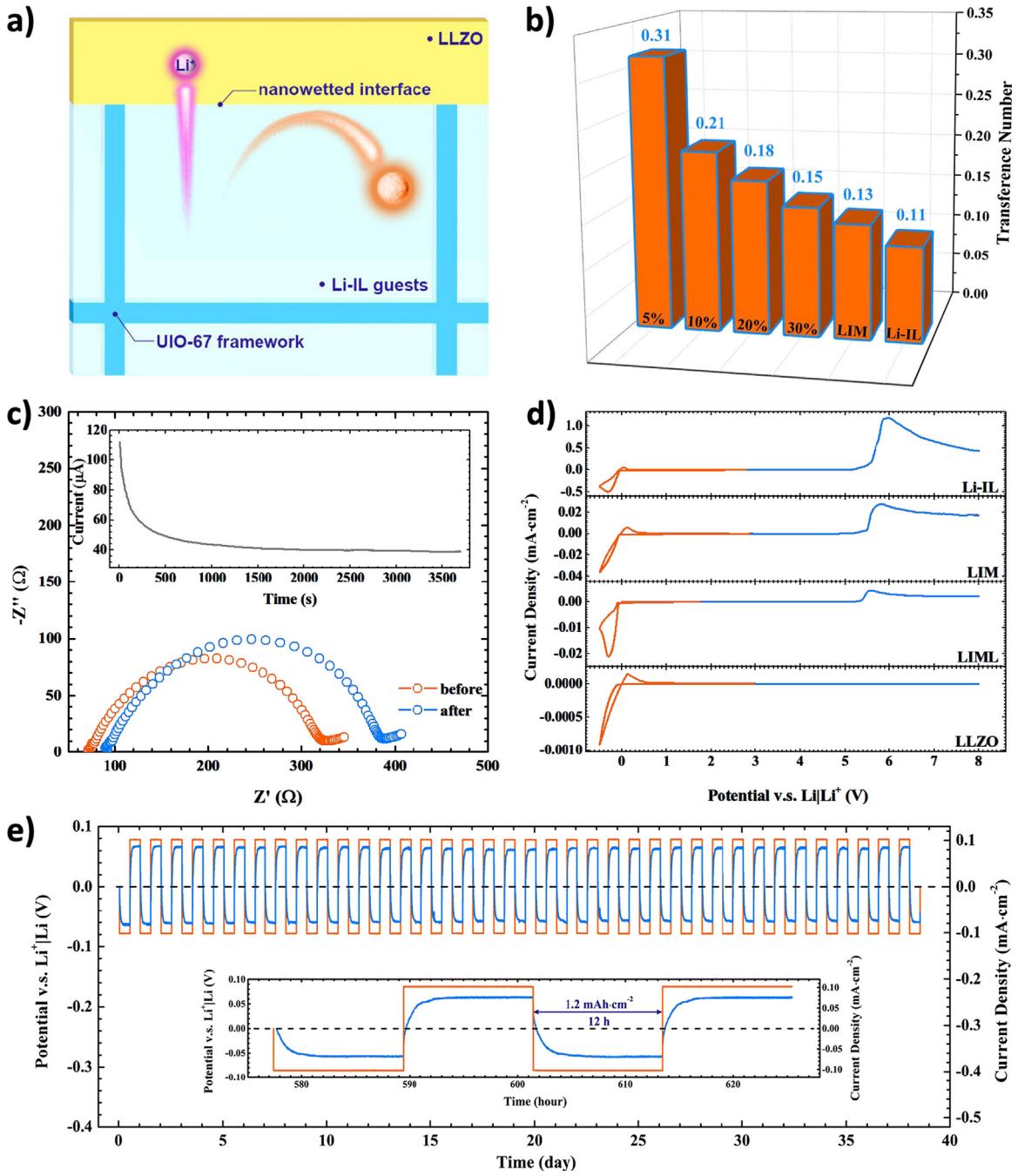

Fig. 3. a) Schematic illustration for the nanowetted interfacial mechanism. Li^+ ions and other ions in Li-IL are presented by pink and orange spheres, respectively. b) Li^+ transference numbers of pristine Li-IL, LIM ionic conductor, and the LIM-L hybrid SSEs with different compositions. c) EIS of the Li|LIM-L|Li (containing 20 wt% of LIM) symmetric cell before and after polarization, inset: variation of current with time during polarization at an applied voltage of 10 mV at room temperature. d) Electrochemical windows of pristine Li-IL, pristine LLZO, LIM ionic conductor and LIM-L hybrid SSE with a scan speed of 0.2 mV s^{-1} at room temperature. e) Li plating-stripping performance of the Li|LIM-L|Li symmetric cell under a current density of 0.1 mA cm^{-2} with a deposition amount of 1.2 mAh cm^{-2} for each half cycle at room temperature.

speculated was caused by the interactions between the MOF host and the large $[EMIM]^+$ and $[TFSI]^-$ guest ions [31]. Theoretically, the t_{Li+} of LLZO SSE is 1, and it dropped to 0.31, 0.21, 0.18, and 0.15 upon mixing with 5 wt%, 10 wt%, 20 wt%, and 30 wt% of LIM, respectively. A low t_{Li+} implies poor rate performance and limited power output of the SSBs. So on the basis of an applicable ionic conductivity, the LIM content in LIM-L should be kept low and thus 20 wt% LIM with 80 wt% LLZO was chosen as an optimized composition for LIM-L hybrid SSE. The EIS results before and after polarization with the potentiostatic polarization current curve to calculate t_{Li+} of this sample are displayed in Fig. 3**c**. The significantly increased ionic conductivity of the LIM-L hybrid SSEs proved that the LIM ionic conductor could effectively reduce the interfacial resistance of LLZO SSE as indicated by the much smaller semicircle of its EIS diagram in Fig. 2**d** compared with that of pristine LLZO (Fig. S5). SEM image for the cross-section view of LIM-L hybrid SSE is shown in Fig. S6. The gaps between the micron-sized LLZO grains were fully filled with nano-sized LIM crystals which acted as "highways" for the Li^+ transport between LLZO grains. The crystal structure of MOF host was an open 3D scaffold and the Li-IL ions inside could directly make contact with the surface of LLZO grains through the

open tunnels of LIM crystals and thus the LIM-LLZO interface was actually wetted with the Li-IL guest at atomic scale. In pristine LLZO SSE, the energy barrier was high for Li^+ ions to go across the solid-solid interface from one LLZO grain lattice into another. But in LIM-L hybrid SSE, such Li^+ transport became much easier. The Li^+ ions at the surface of one LLZO grain were firstly "solvated" by $[TFSI]^-$ ions, and then went into LIM where equal amount of Li ions was "desolvated" and intercalated into another LLZO grain at the same time [32]. The whole interfacial process was just like that in a liquid electrolyte system which was fast and favored the Li^+ transport inside the LIM-L hybrid SSE. Such "nanowetted" interfacial mechanism is schematically illustrated in Fig. 3**a**. The contribution of LLZO main body to the high conductivity of LIM-L was also studied by comparing with an Al_2O_3-LIM mixture. 80 wt % α-Al_2O_3 with similar particle size to the LLZO powders was combined with 20 wt% LIM ionic conductor, and was pressed into pellets to perform conductivity test. According to the EIS in Fig. S7, the mixture represented a low ionic conductivity of about 4.3×10^{-6} S cm^{-1} at 30 °C, indicating that the LLZO with a high bulk conductivity also played an essential role in the high conductivity of the LIMIL hybrid SSE. LLZO has been reported to be stable against ionic liquid species [28], and the chemical stability of the nanowetted interfaces in this work was further confirmed by the wide electrochemical window (EW) of the LIM-L hybrid SSE. The EWs of Li-IL, LLZO, LIM and LIM-L were tested using Li asymmetric cells with an inert stainless steel electrode. As shown in Fig. 3**d**, pristine LLZO showed a very high oxidation potential over 8 V [27,33] and Li-IL began to decompose when the voltage scanned to 5.2 V. The EWs of LIM and LIM-L were also determined to be 5.2 V, providing additional evidence for the high chemical stability of the Li-IL-MOF-LLZO ternary system, which were adequate to the applications of high energy density SSBs containing high-voltage cathodes.

One important feature of the ceramic SSEs is their ability to block Li dendrites, which enables the use of Li metal anode in SSBs to achieve higher energy densities. However, the compatibility of pristine LLZO SSE and Li metal is very poor due to the loose contact with micro-gaps [13,14]. The closely contacted LLZO micro-particles and LIM nanoparticles can be expected to effectively block the growth of Li dendrites. Benefitted from the nanowetted interfacial mechanism of the LIM ionic conductor, LIM-L hybrid SSE exhibited a significantly improved compatibility with Li metal. To examine the reliability of LIM-L hybrid SSE for lithium SSBs, Li|LIM-L|Li symmetric cell was assembled for the galvanostatic Li plating-stripping test at a current density of 0.1 mA cm^{-2} and a deposition amount of 1.2 mAh cm^{-2} at room temperature. As shown in Fig. 3**e**, the polarization voltage of the symmetric cell was about 60 mV, which was stabilized over 12 h for each half cycle with a smooth profile. Moreover, after about 40 days cycling, no short-circuit was observed on the cell and the polarization voltage was nearly unchanged for each cycle. These results implied a small interfacial resistance and a stable interface of LIM-L hybrid SSE against Li metal and also confirmed its ability to block Li dendrite growth under a large Li deposition amount. As a comparison, without LIM ionic conductor, the Li|LLZO|Li symmetric cell demonstrated a fluctuating potential with large voltage polarization (Fig. S8) indicating an unstable Li^+ transport through the interfaces. To better understand the function of LIM in the stable Li plating-stripping process, the Li|LIM-L|Li cell was disassembled after cycling, and the Li metal was washed with fresh dimethyl carbonate (DMC) and then examined by SEM. As shown in Fig. S9**a**, the surface of Li metal anode after cycling was still flat and smooth without vertical dendrites. At higher magnification (Fig. S9b and S9c), a homogenous Li deposition layer could be distinguished, which was composed by many plate-like nanostructures. Obviously, the vertical growth of these nanostructures was depressed by the hybrid SSE layer and such homogenous Li deposition would effectively protect the battery form short circuit. The composition of the deposition layer was further studied by X-ray photoelectron spectrometer (XPS). As displayed in Figs. S9d and S9e, the S and F elements belonging to the Li-IL were detected on the surface, indicating a solid electrolyte interphase (SEI) formed on the Li deposition layer, which was probably caused by the decomposition of IL ions.

Due to the limited ionic transport within the cathode material, carbon, and binder, the interfacial issue in the cathode region of SSBs is much more crucial. Here, the LIM ionic conductor with nanowetted interfaces was used in the cathode instead of conventional SSEs. SSBs with commercial $LiCoO_2$ and $LiFePO_4$ were assembled and tested to demonstrate the capability of LIM to favor the Li^+ transport. Typically, the cathode material was mixed with desired amount of LIM ionic conductor and acetylene black as the cathode mixture, which was sequentially pressed with LIM-L hybrid SSE into a double-layer membrane. Li metal foil was used directly as the anode. Fig. S10 demonstrates the SEM image with corresponding energy dispersive spectrometer (EDS) elemental mappings for the double-layer structure of LCO SSB. The seamlessly laminated LCO cathode and LIM-L hybrid SSE could be clearly distinguished, which were about 139 μm and 120 μm in thickness, respectively. In the cathode part, LCO particles were homogeneously surrounded by LIM and acetylene black forming 3D-connected networks which implied both good ionic and electronic conductivity. The LCO active loading was as high as 15.9 mg cm^{-2} with a cathode composition of 50 wt% LCO, 40 wt% LIM, and 10 wt% acetylene black. Similar results could be observed on the LFP SSB with an active loading of 12.4 mg cm^{-2}, as shown in Fig. S11. Fig. 4 displays the battery performance of the SSBs. At 0.1 C (1 C = 140 mA g^{-1} for LCO, and 170 mA g^{-1} for LFP) current rate, discharge capacities of about 130 and 140 mAh·g^{-1} were observed on the LCO and LFP SSBs, respectively, and they dropped to 33 and 37 mAh·g^{-1} when the current rate was increased to 0.8 C. The room-temperature rate performance of the SSBs was inferior to their LIB counterparts with liquid electrolyte due to the relatively high polarization as indicated by the charge-discharge profiles, which can be further improved by optimizing the cathode composition and reducing the LIM-L hybrid SSE thickness in the future. For long-term cycling at 0.1 C rate, both of the LCO and LFP SSBs showed excellent cyclability with capacity retention of about 97% over 150 cycles and the capacity degradation was 0.29‰ and 0.27‰ for each cycle, respectively. The Coulombic efficiency for the first cycle of LCO and LFP SSBs was 94% and 97%, respectively, which increased to about 98% in the following cycles. The relatively large irreversible capacity fading of LCO cathode in the first cycle was probably caused by the formation of passivation layer at the LCO/LIM interfaces due to the high charge voltage [34,35]. Such a good battery performance could be hardly achieved by the SSBs without LIM ionic conductor. As the LIM in the cathode part was replaced with an equal amount of LLZO, the SSB revealed almost no discharge capacity according to our experiment result, which is caused by the large inner resistance. The superior cycling performance of the SSBs was ascribed to the presence of the LIM ionic conductor, which could establish abundant nanowetted interfaces around solid particles including LLZO and cathode to boost overall Li^+ transport. Based on the battery performance in this work, the specific energy and energy density were calculated with optimized parameters (**Tab. S1** and **Tab. S2**), delivering 196.9 Wh kg^{-1} and 377.0 Wh L^{-1} for LCO battery and 151.3 Wh kg^{-1} and 304.1 Wh L^{-1} for LFP battery, demonstrating such a configuration of SSB with LIM ionic conductor is promising for practical applications. The active loadings and cycle performance in this work were further compared with the recently reported SSBs, which were summarized in **Tab. S3**.

4. Conclusions

In this work, a novel ionic conductor was designed by impregnating a Li^+ containing ionic liquid into a MOF host and was used in the LLZO based solid-state batteries to reduce the interfacial resistance. The MOF host featuring an open 3D scaffold crystal structure enabled the direct contact of inner solidified Li-IL with LLZO and cathode particles to form the "nanowetted" interfaces and favored the interfacial Li^+ transport.

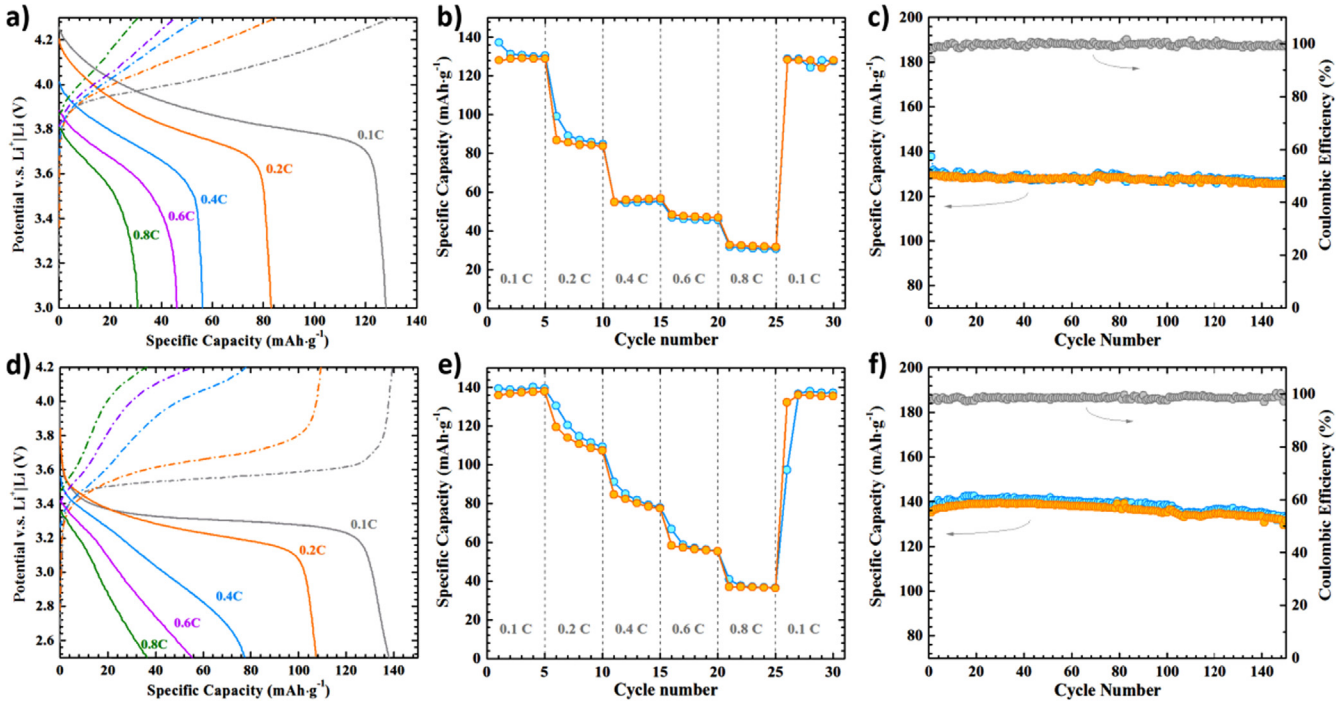

Fig. 4. a) Charge-discharge profiles under different current rates, b) the rate capability, and c) the cycle performance at 0.1 C with Coulombic efficiency of the $LiCoO_2$ SSBs. d) Charge-discharge profiles under different current rates, e) the rate capability, and f) the cycle performances at 0.1 C with Coulombic efficiency of the $LiFePO_4$ SSBs. All the battery tests were performed at room temperature.

The hybrid SSE composed by the ionic conductor and LLZO demonstrated a high ionic conductivity of 1.0×10^{-4} S cm^{-1} with a wide chemical window of 5.2 V. The hybrid SSE also exhibited good compatibility with Li metal anode owing to the nanowetted interfacial mechanism and the Li dendrite growth could be effectively diminished by the homogenous Li deposition. When the ionic conductor was introduced to the LCO and LFP SSBs, efficient Li^+ transport networks were established inside the batteries leading to acceptable rate capability and excellent cyclability. The unique concept for the assistant ionic conductor with "nanowetted" interfaces to boost interfacial Li^+ transport we proposed here is an alternative way to realize the up-scale manufactures and applications of SSBs.

Acknowledgements

This work was financially supported by National Materials Genome Project (2016YFB0700600), the National Natural Science Foundation of China (51672012), Shenzhen Science and Technology Research Grant (JCYJ20150729111733470, JCYJ20151015162256516), and China Postdoctoral Science Foundation (2017M620520, 2017M620497).

Appendix A. Supporting information

Supplementary data associated with this article can be found in the online version at http://dx.doi.org/10.1016/j.nanoen.2018.04.076.

References

[1] M.V. Reddy, G.V. Subba Rao, B.V.R. Chowdari, Chem. Rev. 113 (2013) 5364–5457.
[2] W. Li, B. Song, A. Manthiram, Chem. Soc. Rev. 46 (2017) 3006–3059.
[3] P.G. Bruce, S.A. Freunberger, L.J. Hardwick, J.M. Tarascon, Nat. Mater. 11 (2012) 19–29.
[4] Y. Liu, P. He, H. Zhou, Adv. Energy Mater. 8 (2017) 1701602.
[5] H. Wang, D. Lin, Y. Liu, Y. Li, Y. Cui, Sci. Adv. 3 (2017) 1701301.
[6] X. Yao, B. Huang, J. Yin, G. Peng, Z. Huang, C. Gao, D. Liu, X. Xu, Chin. Phys. B 25 (2016) 018802.
[7] C. Sun, J. Liu, Y. Gong, D.P. Wilkinson, J. Zhang, Nano Energy 33 (2017) 363–386.
[8] L. Yang, Z. Wang, Y. Feng, R. Tan, Y. Zuo, R. Gao, Y. Zhao, L. Han, Z. Wang, F. Pan, Adv. Energy Mater. 7 (2017) 1701437.
[9] L. Chen, Y. Li, S. Li, L. Fan, C. Nan, J.B. Goodenough, Nano Energy 46 (2018) 176–184.
[10] J. van den Broek, S. Afyon, J.L.M. Rupp, Adv. Energy Mater. 6 (2016) 1600736.
[11] J.F. Wu, W.K. Pang, V.K. Peterson, L. Wei, X. Guo, ACS Appl. Mater. Interfaces 9 (2017) 12461–12468.
[12] Z. Wang, R. Tan, H. Wang, L. Yang, J. Hu, H. Chen, F. Pan, Adv. Mater. 30 (2017) 1704436.
[13] K. Fu, Y. Gong, B. Liu, Y. Zhu, S. Xu, Y. Yao, W. Luo, C. Wang, S.D. Lacey, J. Dai, Y. Chen, Y. Mo, E. Wachsman, L. Hu, Sci. Adv. 3 (2017) 1601659.
[14] X. Han, Y. Gong, K. Fu, X. He, G.T. Hitz, J. Dai, A. Pearse, B. Liu, H. Wang, G. Rubloff, Y. Mo, V. Thangadurai, E.D. Wachsman, L. Hu, Nat. Mater. 16 (2017) 572–579.
[15] C. Wang, Y. Gong, B. Liu, K. Fu, Y. Yao, E. Hitz, Y. Li, J. Dai, S. Xu, W. Luo, E.D. Wachsman, L. Hu, Nano Lett. 17 (2017) 565–571.
[16] H. Chen, H. Tu, C. Hu, Y. Liu, D. Dong, Y. Sun, Y. Dai, S. Wang, H. Qian, Z. Lin, L. Chen, J. Am. Chem. Soc. 140 (2018) 896–899.
[17] B.M. Wiers, M.L. Foo, N.P. Balsara, J.R. Long, J. Am. Chem. Soc. 133 (2011) 14522–14525.
[18] R. Ameloot, M. Aubrey, B.M. Wiers, A.P. Gómora-Figueroa, S.N. Patel, N.P. Balsara, J.R. Long, Chem. Eur. J. 19 (2013) 5533–5536.
[19] K. Fujie, R. Ikeda, K. Otsubo, T. Yamada, H. Kitagawa, Chem. Mater. 27 (2015) 7355–7361.
[20] R. Chen, J. Zhang, J. Chelora, Y. Xiong, S.V. Kershaw, K.F. Li, P.K. Lo, K.W. Cheah, A.L. Rogach, J.A. Zapien, C.S. Lee, ACS Appl. Mater. Interfaces 9 (2017) 5699–5708.
[21] Z. Hu, H. Liu, H. Ruan, R. Hu, Y. Su, L. Zhang, Ceram. Int. 42 (2016) 12156–12160.
[22] J.H. Cavka, S. Jakobsen, U. Olsbye, N. Guillou, C. Lamberti, S. Bordiga, K.P. Lillerud, J. Am. Chem. Soc. 130 (2008) 13850–13851.
[23] M. Watanabe, M.L. Thomas, S. Zhang, K. Ueno, T. Yasuda, K. Dokko, Chem. Rev. 117 (2017) 7190–7239.
[24] M. Armand, F. Endres, D.R. MacFarlane, H. Ohno, B. Scrosati, Nat. Mater. 8 (2009) 621–629.
[25] S. Seki, Y. Kobayashi, H. Miyashiro, Y. Ohno, A. Usami, Y. Mita, N. Kihira, M. Watanabe, N. Terada, J. Phys. Chem. B 110 (2006) 10228–10230.
[26] K. Fujie, T. Yamada, R. Ikeda, H. Kitagawa, Angew. Chem. Int. Ed. 53 (2014) 11302–11305.
[27] T. Thompson, S. Yu, L. Williams, R.D. Schmidt, R. Garcia Mendez, J. Wolfenstine, J.L. Allen, E. Kioupakis, D.J. Siegel, J. Sakamoto, ACS Energy Lett. 2 (2017) 462–468.
[28] H.W. Kim, P. Manikandan, Y.J. Lim, J.H. Kim, S.C. Nam, Y. Kim, J. Mater. Chem. A 4 (2016) 17025–17032.
[29] J. Evans, C.A. Vincent, P.G. Bruce, Polymer 28 (1987) 2324–2328.
[30] M. Galiński, A. Lewandowski, I. Stępniak, Electrochim. Acta 51 (2006) 5567–5580.
[31] H. Choi, H.W. Kim, J.K. Ki, Y.J. Lim, Y. Kim, J.H. Ahn, Nano Res. 10 (2017) 3092–3102.
[32] O. Borodin, G.D. Smith, W. Henderson, J. Phys. Chem. B 110 (2006) 16879–16886.

[33] S. Song, D. Sheptyakov, A.M. Korsunsky, H.M. Duong, L. Lu, Mater. Des. 93 (2016) 232–237.
[34] S. Kang, W. Yoon, K. Nam, X. Yang, D.P. Abraham, J. Mater. Sci. 43 (2008) 4701–4706.
[35] J. Kasnatscheew, M. Evertz, B. Streipert, R. Wagner, R. Klopsch, B. Vortmann, H. Hahn, S. Nowak, M. Amereller, A.C. Gentschev, P. Lamp, M. Winter, Phys. Chem. Chem. Phys. 18 (2016) 3956–3965.

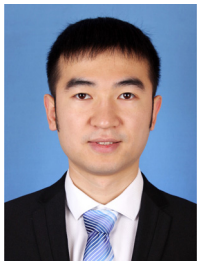

Ziqi Wang received his Ph.D. degree under the supervision of Prof. Guodong Qian at Zhejiang University (China) in 2016. Dr. Wang is currently a postdoctoral researcher at the School of Advanced Materials, Peking University Shenzhen Graduate School (China) in Prof. Feng Pan's group. His research interests focus on the metal-organic frameworks (MOFs) and their applications in electrochemical energy storage

Zijian Wang received his B.S. degree from the School of Materials Science and Engineering at Nanchang University (China) in 2016. Wang is now pursuing his Ph.D. degree under the supervision of Prof. Feng Pan at the School of Advanced Materials, Peking University Shenzhen Graduate School, China. His research interests focus on developing novel solid-state electrolytes for all-solid-state Li batteries.

Luyi Yang received his Ph.D. degree from the School of Chemistry at Southampton University in 2015 under the supervision of Prof. John Owen. Dr. Yang is currently a postdoctoral researcher at the School of Advanced Materials, Peking University Shenzhen Graduate School. His research interests mainly focus on designing key components for solid-state batteries.

Hongbin Wang received his B.S. degree from the School of Materials Science and Engineering at Jilin University (China) in 2009, and earned Ph.D. degree from the School of Chemistry at Jilin University in 2015 under the supervision of Prof. Zongtao Zhang. Dr. Wang is now pursuing his postdoctoral training with Prof. Feng Pan at the School of Advanced Materials, Peking University Shenzhen Graduate School, China. His research interests mainly lie in exploring key materials and technologies for energy storage and conversion applications including lithium ion batteries, sodium ion batteries, and supercapacitors.

Yongli Song was born in Harbin, China. He received the B.S. degree (2010) in Optics and the M.S. degree (2013) in Condensed Matter Physics from Harbin Institute of Technology (HIT), China. In 2017, he received his Ph.D. degree in Prof. Y. Sui's group at the department of physics, HIT. He is now working as a postdoctoral researcher in Prof. F. Pang group. His current research is focused on lithium-based batteries.

Han Lei received his B.S. degree in 2016 from Peking University, China. He is pursuing his M.S. degree in the School of Advanced Materials, Peking University Shenzhen Graduate School, China. His research interests include advanced functional materials and their new application in energy storage and conversion devices, such as all solid-state batteries, conductive polymers, and so on.

Kai Yang received his B.S. degree in the School of Aerospace from Tsinghua University in 2016, China. He is pursuing his M.S. degree in the School of Advanced Materials, Peking University Shenzhen Graduate School, China. His main research interests include advanced silicon carbon materials for lithium ion batteries (LIBs) and advanced technology for interface research in LIBs such as in-situ AFM and EQCM.

Jiangtao Hu received his B.S. degree from Henan University in 2013, China. Hu is now pursuing his Ph.D. degree under the supervision of Prof. Feng Pan at the School of Advanced Materials, Peking University Shenzhen Graduate School, China. His research interests mainly lie in design and development of functional materials for energy storage and conversion applications such as batteries, supercapacitors, and catalysis.

Haibiao Chen is currently a senior researcher at the School of Advanced Materials, Peking University Shenzhen Graduate School (China). He received his Bachelor's degree from Tsinghua University (China) in 2000 and Ph.D. from Stevens Institute of Technology (USA) in 2006. He worked at Velocys (USA) during 2006-2011 and UES (USA) during 2011-2014 prior to joining Peking University Shenzhen Graduate School.

Feng Pan, founding Dean of School of Advanced Materials, Peking University Shenzhen Graduate School, got B.S. from Dept. Chemistry, Peking University in 1985 and Ph.D. from Dept. of P&A Chemistry , University of Strathclyde, Glasgow, UK, with "Patrick D. Ritchie Prize" for the best Ph.D. in 1994. With more than a decade experience in large international incorporations, Prof. Pan has been engaged in fundamental research and product development of novel optoelectronic and energy storage materials and devices. As Chief Scientist, Prof. Pan led eight entities in Shenzhen to win 150 million RMB grant for the national new energy vehicles (power battery) innovation project since 2013.